

Pathological tau spreads through communicating brain regions in human Alzheimers disease

Jacob W. Vogel^{a,*}, Yasser Iturria-Medina^a, Olof T. Strandberg^b, Ruben Smith^b, Alan C. Evans^{a,**}, Oskar Hansson^{b,c,**}, for the Alzheimer's Disease Neuroimaging Initiative, and the Swedish BioFinder Study

^a*Montreal Neurological Institute, McGill University, Montréal, QC, Canada*

^b*Clinical Memory Research Unit, Lund University, Lund, Sweden*

^c*Memory Clinic, Skne University Hospital, Lund, Sweden*

Abstract

Tau is one of the two pathological hallmarks of Alzheimer's disease, and bears a much closer relationship to local neurodegeneration and cognitive impairment than the other hallmark, β -amyloid. Cell and rodent models have shown evidence that tau spreads from cell to cell through anatomical neuronal connections, and that this process is facilitated by the presence of β -amyloid. We test this hypothesis in humans by using an epidemic spreading model (ESM) to simulate the spread of tau over human neuronal connections, and we compare the simulated pattern of progression to the observed pattern measured in the brains of 295 individuals on the Alzheimer's disease spectrum, using PET. Fitting our model, we found that the majority of variance in the overall pattern of tau progression could be explained by diffusion of an agent through the human connectome, measured using either functional connectivity or diffusion tractography. These models far exceeded chance, and outperformed models testing the extracellular spread of tau over Euclidian space. Surprisingly, the ESM predicted the spatial patterns of sub-threshold

*Corresponding authors: jacob.vogel@mail.mcgill.ca, alan.evans@mcgill.ca

**These authors contributed equally to the work

Data used in preparation of this article were obtained from the Alzheimer's Disease Neuroimaging Initiative (ADNI) database (adni.loni.usc.edu). As such, the investigators within the ADNI contributed to the design and implementation of ADNI and/or provided data but did not participate in analysis or writing of this report. A complete listing of ADNI investigators can be found at: <http://adni.loni.usc.edu/wp-content/uploads/howtoapply/ADNIAcknowledgementList.pdf>

tau in cognitively normal elderly without significant amyloid burden with impressive accuracy. In addition, in amyloid-positive subjects only, regions with greater amyloid burden showed greater tau than predicted by connectivity patterns, suggesting a role of amyloid in accelerating the spread of tau in certain isocortical regions. Altogether, our results provide strong evidence that tau spreads through neuronal communication pathways even in normal aging, and that this process is accelerated by the presence of brain β -amyloid.

Keywords: tau, PET, diffusion models, connectivity, alzheimer's disease, brain networks

1. Introduction

Alzheimer's disease is characterized by the presence of β -amyloid plaques and neurofibrillary tangles of hyper-phosphorylated tau at autopsy. Both of these pathological phenomena can now be quantified spatially in the brains of living humans using positron emission tomography (PET), allowing for the study of disease progression before death and, indeed, before symptoms manifest [1]. β -amyloid plaques are detectable in the brain many years or even decades before dementia onset [2], but appear to have only subtle effects on cognition and brain health [3, 4, 5, 6], if any. In contrast, tau neurofibrillary tangles are strongly correlated with local neurodegeneration and, in turn, cognitive impairment [7, 8]. However, tau tangle aggregation in the medial temporal lobes is a normal and fairly innocuous feature of normal aging [9, 10, 11]. Frank cognitive impairment often coincides with the spreading of NFTs out of the medial temporal lobes and into the surrounding isocortex **cite**, a process that animal models have suggested may be potentiated or accelerated by the presence of β -amyloid plaques [12, 13].

Due to its close link with neurodegeneration and cognitive impairment, tau has received special attention as a potential therapeutic target for Alzheimer's disease [14]. Perhaps the most compelling features of tau pathophysiology are its rather focal distribution of aggregation and its highly stereotyped pattern of progression through the brain. Specifically, neurofibrillary tangles first appear in the transentorhinal cortex, before spreading to the anterior hippocampus, followed by adjacent limbic and temporal cortex, association isocortex, and finally to primary sensory cortex [15, 10, 16, 17]. This very particular pattern has lead many to speculate that pathological tau itself, or a pathological process that incurs tau hyper-phosphorylation and toxicity,

27 may spread directly from cell to cell through anatomical connections [18, 19].
28 Strong evidence in support of this hypothesis has come from animal models,
29 which have repeatedly demonstrated that human tau injected into the brains
30 of β -amyloid expressing transgenic rodents leads to the aggregation of tau in
31 brain regions anatomically connected to the injection site [20, 21, 22, 23, 12].
32 An important caveat to the aforementioned studies is that they involve in-
33 jection of tau aggregates that greatly exceed the amount of tau produced in
34 naturally in the brain. In addition, the studies were performed in animals
35 that do not get Alzheimer’s disease naturally. This latter point is especially
36 important, as some of the largest differences in the gene expression profiles
37 of rodent and human brains include many proteins linked to Alzheimer’s dis-
38 ease [24], suggesting important differences in the neural environment between
39 mice and humans. In addition, the success of many therapies in rodents have
40 failed to translate to humans [25], suggesting a need to test the hypothesis
41 of anatomical tau-spreading directly in humans.

42 Unfortunately, there are many obstacles to studying the tau-spreading
43 hypothesis in humans. While autopsy studies have provided evidence for tau
44 spreading [26, 27], this evidence comes in the form of limited snapshots in
45 deceased individuals. Tau-PET allows for the quantification of tau *in vivo*,
46 but the PET signal is contaminated by off-target binding that limit interpre-
47 tations [28, 29, 30, 31]. Despite this limitation, circumstantial evidence has
48 emerged supporting the hypothesis that tau spreads through connected neu-
49 rons in humans. Studies decomposing the spatial distribution of tau-PET
50 signal in the human brain have revealed spatial patterns highly reminis-
51 cent of brain functional networks [32, 33]. In addition, brain regions with
52 greater functional connections to the rest of the brain tend to have greater
53 tau accumulation [34], and correlations have been found between whole-brain
54 functional connectivity and whole-brain tau covariance [35]. Finally, changes
55 in white matter bundles between two specific regions predicted spreading
56 dynamics between those regions [36]. We test the tau-spreading hypothesis
57 more directly by placing a “tau seed” in the entorhinal cortex, simulating
58 its diffusion through measured functional and anatomical connections, and
59 comparing the simulated pattern of global tau spread with actual pattern
60 derived from tau-PET scans of 295 individuals. This method allows for a
61 cascade of secondary tau seeding events to occur along a network over time,
62 more closely simulating proposed models of tau spread in the brain. Similar
63 models have been employed to successfully describe spreading patterns of β -
64 amyloid in Alzheimer’s disease [37], as well as atrophy patterns in Alzheimer’s

	CN	MCI	AD	Total
n	175	57	63	195
Age (SD)	72.0 (6.3)	71.31 (8.6)	71.9 (8.2)	71.8 (7.2)
% Women	56.0%	38.6%	42.9%	49.8%
Education (SD)	14.9 (3.6)	14.4 (3.6)	13.0 (3.9)	14.4 (3.7)
% ApoE4	41.4%	82.5%	68.4%	55.7%
% Amyloid Positive	42.6%	100.0%	98.3%	66.2%

65 disease other dementias [38, 39]. Our analysis also improves upon these and
66 other prior studies by introducing a method for increasing the fidelity of tau-
67 PET signal using regional mixture-modeling, and by incorporating post-hoc
68 information related to β -amyloid pathology.

69 2. Methods

70 2.1. Participants

71 Participants of this study represented a selection of individuals from two
72 large multi-center studies: the Swedish BioFinder Study (BioF; <http://biofinder.se/>)
73 and the Alzheimer’s Disease Neuroimaging Initiative (ADNI; adni.loni.usc.edu).
74 Both studies were designed to accelerate the discovery of biomarkers indi-
75 cating progression of Alzheimer’s disease pathology. Participants were se-
76 lected based on the following inclusion criteria: participants must i) have
77 an AV1451-PET scan, ii) have either an β -amyloid-PET scan (for ADNI:
78 [^{18}F]-Florbetapir, for BioF: [^{18}F]-Flutemetamol) or CSF β -amyloid1-42 indi-
79 cating amyloid-status. In addition, participants were required to be cog-
80 nitively unimpaired, or have a clinical diagnosis of mild cognitive impairment or
81 Alzheimer’s dementia with biomarker evidence of β -amyloid positivity. For
82 both cohorts separately, β -amyloid positivity was defined using a previously
83 described mixture modeling procedure [5]. For BioFINDER, β -amyloid1-42
84 positivity was defined as an (INNOTEST) level below 650ng/L [40]. All
85 ADNI participants fitting the inclusion criteria with AV1451 scans acquired
86 (BioFINDER) or who were available for public download (ADNI) in May
87 2018 were included in this study. In total across both studies, 175 cognitively
88 unimpaired individuals (69 amyloid-positive), 57 amyloid-positive individu-
89 als with mild cognitive impairment and 63 amyloid-positive individuals with
90 suspected Alzheimers dementia were included. Demographic information can
91 be found in Table 1.

92 *2.2. PET Acquisition and Pre-processing*

93 MRI and PET acquisition procedures for ADNI (<http://adni.loni.usc.edu/methods/>)
94 and BioF [41] have both been previously described at length. All AV1451-
95 PET scans across studies were processed using the same pipeline, which has
96 also been previously described [41, 33]. Briefly, 5-min frames were recon-
97 structed from 80-100 minutes post-injection. These frames were re-aligned
98 using AFNIs 3dvolreg (<https://afni.nimh.nih.gov/>) and averaged, and the
99 mean image was coregistered to each subject’s native space T1 image. The
100 coregistered image was intensity normalized using an inferior cerebellar gray
101 reference region, creating standard uptake value ratios (SUVR).

102 *2.3. Transformation of PET data to regional probabilities*

103 Mean regional tau-PET SUVRs were extracted from each individual’s
104 native space PET image using the Desikan-Killiany atlas [42], an 83-region
105 atlas based on structural morphometry. All cerebellar regions were removed
106 from the atlases, leaving 78 regions in total.

107 Previous AV1451-PET studies have noted considerable off-target bind-
108 ing of the AV1451 signal, leading to signal in regions without pathological
109 tau burden, and likely to pollution of signal in regions accumulating tau
110 [28, 29, 31, 33]. While many previous studies have ignored these issues, ac-
111 counting for off-target binding is essential to the current study, as our model
112 cannot distinguish off-target from target signal, and we are not interested
113 in the propagation of off-target signal. To address this issue, we utilized re-
114 gional Gaussian mixture modeling under the assumption that the target and
115 off-target signal across the population are distinct and separable Gaussian
116 distributions.

117 As most individuals do not have tau in most regions, pathological signal
118 should show a skewed distribution across the population, whereas off-target
119 and non-specific signal should be reasonably normally distributed. Such a
120 bimodal distribution has been observed for β -amyloid, and mixture modeling
121 has been used in this context to define global β -amyloid positivity [43, 44].
122 Our approach differs from these previous studies as we do not assume the dis-
123 tribution of target and off-target binding to be homogeneous across cortical
124 areas – we apply Gaussian mixture modeling separately to each region-of-
125 interest (Fig 1A). Specifically, for each region, we fit a one-component and
126 a two-component Gaussian mixture model across the entire population. We
127 compare the fit of the two models using Aikake’s information criterion. If a
128 two-component model fits the data better, this likely indicates the presence

129 of pathological tau in a proportion of the population, and the Gaussians fit
130 to the data provide a rough estimate of an SUVR threshold, above which
131 AV1451 signal has a high probability of being abnormal. If a one-component
132 model fits better, this indicates the AV1451-PET signal within the region
133 is roughly normally distributed across the population, which we do not ex-
134 pect for tau in a population including many cognitively unimpaired indi-
135 viduals. Regions showing a unimodal distribution are therefore discarded
136 from the ESM model, as neurofibrillary tau tangles are likely not expressed
137 in that region within the sample. Furthermore, since the ESM receives re-
138 gional (tau) probabilities as input, we calculate the probability that a given
139 subject's ROI SUVR value falls onto the second (i.e. right-most) Gaussian
140 distribution. Assuming this second distribution represents the subjects with
141 abnormal AV1451 signal, this value estimates the proximity of a subject
142 to the pathological distribution. Effectively, this converts regional SUVRs to
143 tau-positivity probabilities. This approach defines a fairly conservative, data-
144 driven threshold for SUVR values, above which, one can assume the presence
145 of abnormal signal (perhaps indicating pathological tau accumulation) with
146 a high degree of confidence.

147 *2.4. Connectivity measurements*

148 The overall pattern of spread simulated by the ESM is determined by the
149 relationship matrix, which represents pairwise relationships between each
150 region-of-interest. Indeed, this is the system through which the simulated
151 signal will diffuse. Varying the relationship matrix can, for example, allow
152 for the tests of different hypotheses of spread. We use a functional con-
153 nectivity matrix generated from a group of young healthy controls to test
154 the hypothesis that tau spreads through communicating neurons. We vali-
155 date this procedure using anatomical connectivity measurements generated
156 from healthy and impaired older adults. Finally, we test the hypothesis of
157 tau spreading through extra-cellular space by inputting a Euclidian distance
158 matrix as input.

159 Functional connectivity measurements were generated from a subsample
160 of young healthy controls from the COBRE dataset [45], a publicly available
161 sample which we accessed through the Nilearn python library. All subjects
162 listed as healthy controls under the age of 40 were selected, totaling 74 in-
163 dividuals. The images were already preprocessed using the NIAK resting-
164 state pipeline (<http://niak.simexp-lab.org/pipepreprocessing.html>), and ad-
165 ditional details can be found elsewhere [45]. Correlation matrices were gen-

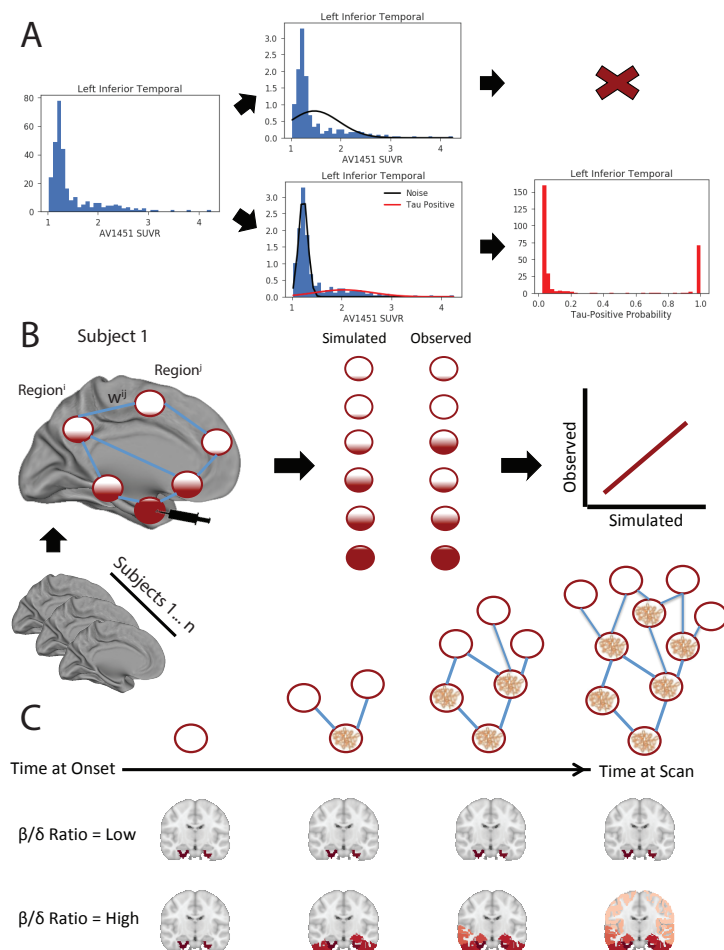


Figure 1: Methodological approaches. A) Summary of the mixture model procedure, using the left inferior temporal lobe as an example. The distribution of all SUVR values in this ROI are shown. Two Gaussian mixture models are fit to the data. When a one-component model first the data better, the ROI is discarded. When a two-component model fits better, the probability that each values falls upon the second distribution is calculated. B) Summary of ESM model. An artificial system based on a pairwise relationship (e.g. functional connectivity) matrix is created, where the relationship between regions i and j is represented by weight w_{ij} . For each subject, a seed is placed at the model epicenter, and the diffusion of this signal over time is simulated through the system, where the inter-regional relationships determine the pattern of spread, and subject-level free parameters determine the velocity of diffusion, until an optimal fit is reached. At this point, the simulated tau signal is compared to the observed tau-PET signal to evaluate the model. C) One advantage of the ESM over traditional approaches lies in the initiation of secondary seeding events as the diffusion process reaches new regions (top). Another advantage lies in the fitting of subject-level production (β) and clearance (δ) parameters. A balance in these parameters will lead to little to no spreading over time, while increasing imbalance leads to increasing speed of spread.

166 erated by finding the correlation between timeseries' of each pair of regions-
167 of-interest from the Desikan-Killiany atlas, and all available confounds were
168 regressed from the correlation matrices. We took the mean of all 74 cor-
169 relation matrices to create an average healthy connectome template. This
170 connectome was then thresholded so as to only retain the top 10% of con-
171 nections, and transformed so all values fell between 0 and 1.

172 To validate our findings, we created a template structural connectiv-
173 ity matrix using DTI tractography data from a non-overlapping sample of
174 healthy and cognitively impaired individuals from ADNI. In total, 204 indi-
175 viduals had one or more DTI scans available, for a total of 540 scans. All
176 scans were preprocessed with a previously described diffusion tractography
177 pipeline [46], and acquisition and processing information has been described
178 in detail [47]. Briefly, orientation distribution functions (ODF) were calcu-
179 lated and in turn used to generate deterministic connections between pairs
180 of brain regions from the Desikan atlas. Specifically, an ACD measure was
181 used, representing the total proportion of regional surface area (across both
182 regions) that contain connecting fibers between the two regions. All images
183 were assessed for quality. Connectomes were averaged across all subjects
184 resulting in a template structural connectome in aging.

185 To create a Euclidian distance matrix, we calculate the coordinate repre-
186 senting the center of mass for each region of interest, and find the Euclidian
187 distance between it and the center of mass of every other ROI. By using this
188 distance matrix in the epidemic spreading model, we test the hypothesis that
189 tau diffuses radially across adjacent cortex, rather than through connected
190 regions.

191 *2.5. The Epidemic Spreading Model*

192 The spread of tau through connected brain regions was simulated us-
193 ing the Epidemic Spreading Model (ESM), a previously described diffusion
194 model that has been applied to explain the spread of β -amyloid through the
195 brain [37]. The ESM simulates the diffusion of a signal from an epicenter
196 through a set of connected regions over time (Fig 1B,C). The dynamics of
197 the spreading pattern are controlled by the weighted connectivity between
198 regions, and by a set of parameters fit within-subject, the latter of which are
199 solved through simulation. Specifically, the parameters represent subject-
200 specific i) global tau production rate, ii) global tau clearance rate and iii)
201 age of onset, which interact with regional-connectivity patterns to determine

202 the velocity of spread. The ESM is fit over time to each subject across sev-
203 eral parameter sets, and the set that produces the closest approximation to
204 observed tau burden for a given subject is selected. Note that these paramete-
205 rs provide no information as to regional patterning, which is the metric by
206 which the accuracy of the model is evaluated (see below). Instead, the free
207 parameters moderate the overall tau burden (i.e. the stopping point), which
208 allows the ESM to be fit to individuals across the Alzheimer’s disease spec-
209 trum. For example, an individual with little-to-no tau burden would likely
210 be fit with a balance of production and clearance rates that would preclude
211 the overproduction and spread of tau signal (1C). A detailed and formalized
212 description of the ESM can be found elsewhere [37].

213 In previous applications of the ESM, the model is fit over every possible
214 epicenter as well as combinations of epicenters, and the epicenter providing
215 the best overall fit to the data is selected. In our case, autopsy work provides
216 strong evidence for a consistent ”epicenter” of tau neurofibrillary tangles in
217 humans. Tangles first emerge in the trans-entorhinal cortex, before emerging
218 in other parts of the entorhinal cortex as well as the anterior hippocampus
219 [15, 10]. We therefore ran models with the left and right entorhinal cortex
220 selected as the model epicenters. However, for the purposes of validation, a
221 best-fitting model-derived epicenter was also computed, by fitting the ESM
222 across all possible regions and finding the best average within-subject fit.
223 Once this epicenter was found, we ran the model once more using both left
224 and right regions as the model epicenters.

225 The ESM takes as input a Region x Subject matrix of values ranging
226 from 0 to 1, representing the probability of a pathological burden (in this
227 case, of tau) in a given region for a given subject. The model is fit within-
228 subject and, for each subject, produces an estimate of tau probability for
229 every region-of-interest.

230 *2.6. Statistical Analysis*

231 The ESM was fit using different relationship matrices (see Section 2.4,
232 above). Each model was evaluated by mean within-individual fit, as well
233 as global population fit. Individual model fit is calculated as the r^2 and
234 mean squared error between predicted regional tau probabilities and actual
235 regional tau probabilities measured with AV1451-PET, for each individual.
236 The mean r^2 across all individuals was used to represent overall model fit.
237 To evaluate the accuracy of the global pattern, the regional predicted and
238 observed tau probabilities, respectively, were averaged across all subjects,

239 and the r^2 and mean squared error between these measures were calculated.
240 These accuracy measures represent the degree to which regional connectivity
241 predicts the spatial pattern of tau-PET measured within and across sub-
242 jects. To ensure the magnitude of our results were greater than chance given
243 a matrix of similar properties, we fit the ESM using 100 null matrices with
244 preserved degree and strength distributions using the Brain Connectivity
245 toolbox (<https://sites.google.com/site/bctnet/>). We use the null distribu-
246 tion to calculate the mean and 95% confidence intervals of the relationship
247 occurring by chance. Since we run only 100 null models per test, the lowest
248 possible p-value is 0.01, which would suggest the observed test value was
249 higher than all values observed by chance.

250 To examine the global accuracy of the ESM stratified by diagnosis, we first
251 divided all subjects into one of four diagnostic groups: amyloid-negative cog-
252 nitively normal (CN-), amyloid-positive cognitively normal (CN+), amyloid-
253 positive MCI (MCI+) and amyloid-positive AD dementia (AD+). We then
254 calculated the mean of predicted and observed values across all subjects
255 within each diagnosis, respectively.

256 Studies in rodents have suggested a role of amyloid in facilitating the
257 rapid fibrillarization of tau oligomers [12]. This would suggest that amyloid
258 may play a role in explaining tau patterns that is at least partially inde-
259 pendent of connectivity patterns. To explore this, we tested the relationship
260 between regional modeling error and regional amyloid depositon. We down-
261 loaded baseline regional β -amyloid SUVR values (using whole-cerebellum) for
262 (N) cognitively normal, MCI and AD subjects from the ADNI website. We
263 converted the SUVR values to amyloid-positive probabilities using the same
264 approach as described in Section 2.3. Next, we used the sign of the residual
265 to divide regions into those that were overestimated by the model, and those
266 that were underestimated by the model. An underestimated region, for ex-
267 ample, would show more tau than the model predicted given that region's
268 connectivity to the model epicenter. We explored the relationship between
269 model estimation and amyloid by comparing the degree amyloid between
270 overestimated and underestimated regions using t-tests. We also examined
271 this relationship separately across clinical diagnoses.

272 3. Results

273 3.1. Conversion to tau-positive probabilities enhances fidelity of tau-PET 274 data

275 Regional mixture modeling of AV1451 SUVR data across all 295 sub-
276 jects suggested a two-component (bimodal) model as a superior fit for all
277 62 cortical regions-of-interest, as well as the left and right hippocampi and
278 amygdalae. For all other subcortical regions-of-interest, a one-component
279 model fit the data better, and these regions were discarded from all further
280 analysis. The remaining 66 regions were converted to tau-positive proba-
281 bilities (Fig 1A). This threshold-free, data-driven transformation yielded a
282 sparse data matrix with a clear pattern suggesting a gradual progression of
283 tau across regions (Fig 2). When sorted from least to most tau (e.g. [16]),
284 the regional ordering greatly resembled the previously described progression
285 of tau pathology [15].

286 3.2. Epidemic spreading of tau over human neuronal connections explains 287 spatial pattern of tau in the brain

288 The epidemic spreading model was fit, simulating the spread of tau signal
289 from a single epicenter through functional brain connections (Fig 3,4). When
290 using the left and right entorhinal cortex as the model epicenter, the model
291 explained 56.5% (null model mean r^2 [95% CI] = 0.060 [0.006, 0.126], $p < 0.01$)
292 of the overall spatial pattern of tau (Fig 4A), and on average, explained 35.6%
293 (SD=21.3%; null model mean r^2 [95% CI] = 0.068 [0.033, 0.147], $p < 0.01$) of
294 the spatial pattern within individual subjects.

295 Next, the ESM was fit allowing the model to select the "best-fitting" re-
296 gional epicenter (Fig 4B). The hippocampus was selected, slightly improving
297 the overall global accuracy of the model to 57.8%, but dramatically increasing
298 the average local (within-subject) explained variance to 46.7% (SD=27.9%).
299 The epidemic spreading model was particularly effective in predicting the
300 early progression of tau, but diverged from the observed tau pattern over
301 time (Fig 3,4).

302 As a validation, the ESM was fit using a structural connectome created
303 using diffusion tensor imaging tractography on a separate sample of healthy
304 and cognitively impaired older adults (Fig 4C). The model fit was highly
305 consistent with models fit over functional connectomes of younger adults.
306 Using a bilateral entorhinal cortex epicenter, the model explained 51.1% (null
307 model mean r^2 [95% CI] = 0.062 [0.020, 0.133], $p < 0.01$) of the overall spatial

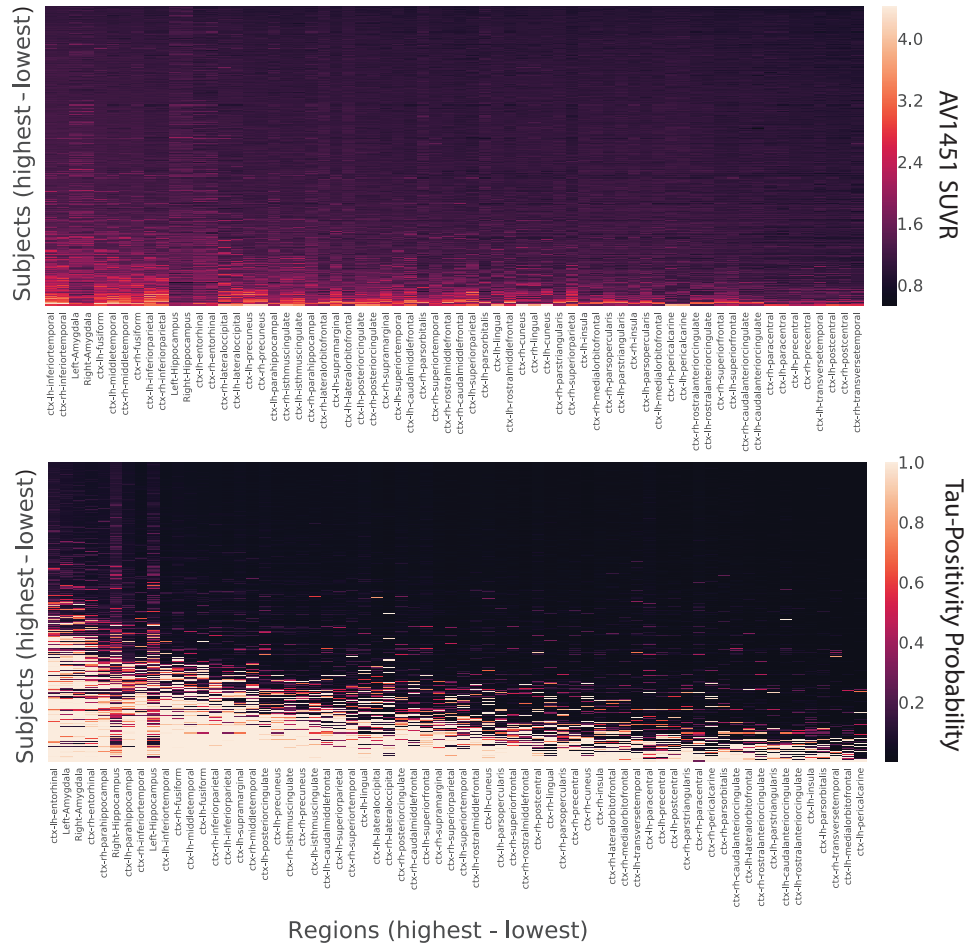


Figure 2: Tau-PET data before and after conversion to tau-positive probabilities. Each row is a subject sorted top-bottom by most to least overall tau. Each column is an ROI, sorted by least to most overall tau. Warmer colors represent higher SUVR values (top) or tau-positive probabilities (bottom). Conversion to tau-positive probabilities creates a sparse distribution of values demonstrating a progression. The order of ROIs resembles those described in the autopsy literature.

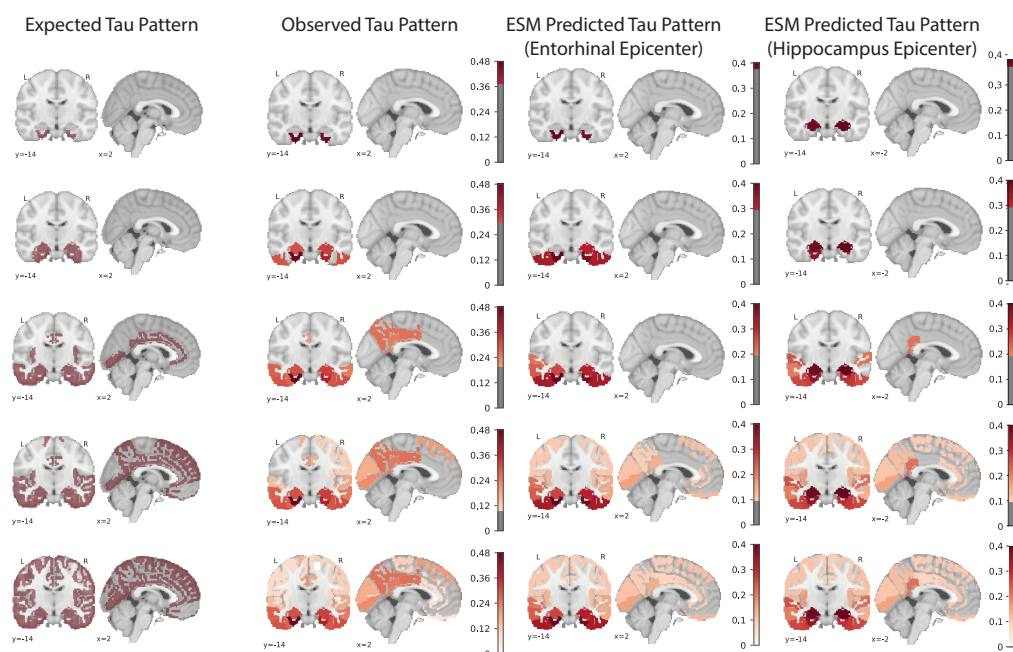


Figure 3: Hypothesized, observed and predicted pattern of tau spreading. (left) Hypothetical spread patterns represented by Braak stages I, II, VI, V and VI as described in [48]. (right) Spreading patterns of (from left to right) the observed tau-PET data, the ESM simulated data with entorhinal epicenter, and with hippocampus epicenter. Warmer colors represent higher proportion of regional tau-positivity predicted or observed across the population. Each "stage" was achieved by arbitrarily thresholding the population-mean tau-positive probability image at the following thresholds: 0.38, 0.3, 0.2, 0.1, 0

308 pattern of tau progression, and on average, explained 37.9% (SD=22.5%, null
 309 model mean r^2 [95% CI] = 0.132 [0.108, 0.186], $p < 0.01$) of the within-subject
 310 variance in tau spatial pattern. Once again, we fit the ESM allowing for a
 311 data-driven epicenter to be selected, and this time, the entorhinal cortex was
 312 selected as the best-fitting epicenter.

313 Alternative hypotheses have been proposed suggesting tau may simply
 314 spread extracellularly across neighboring regions, rather than through anatomical
 315 connections. To test the hypothesis, a model was fit over a Euclidean
 316 distance matrix instead of a functional or structural connectome (Fig 4D).
 317 This model explained considerably less variance, both at the global ($r^2=0.22$)
 318 and individual (mean $r^2=0.20$) level.

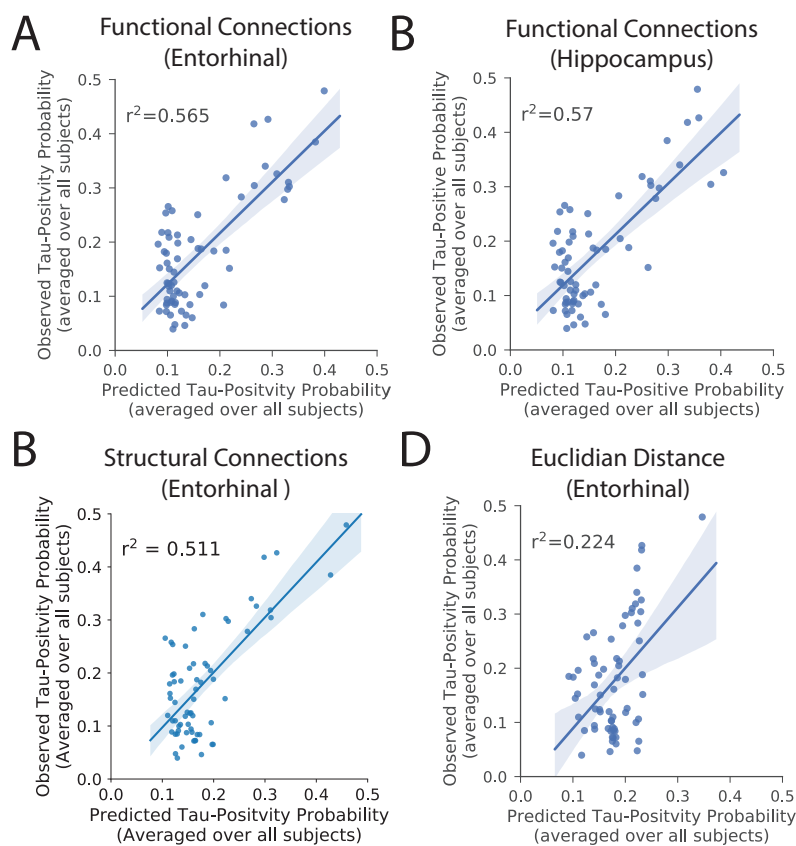


Figure 4: Performance of ESM in predicting spatial progression of tau. For each plot, each dot represents a region. The x-axis represents the mean simulated tau-positive probabilities across the population, while the y-axis represents the mean observed tau-positive probability. A value of (say) 0.3 for a given ROI would suggest that an average of 30% of all subjects included were predicted (X) or observed (Y) to have positive abnormal tau signal in that region. The results are shown for ESM fit over a) healthy functional connectome with entorhinal epicenter; b) healthy functional connectome with a hippocampus epicenter selected as best-fitting; c) aging structural connectome with an entorhinal epicenter (also selected as best-fitting); and d) a Euclidian distance matrix with entorhinal epicenter.

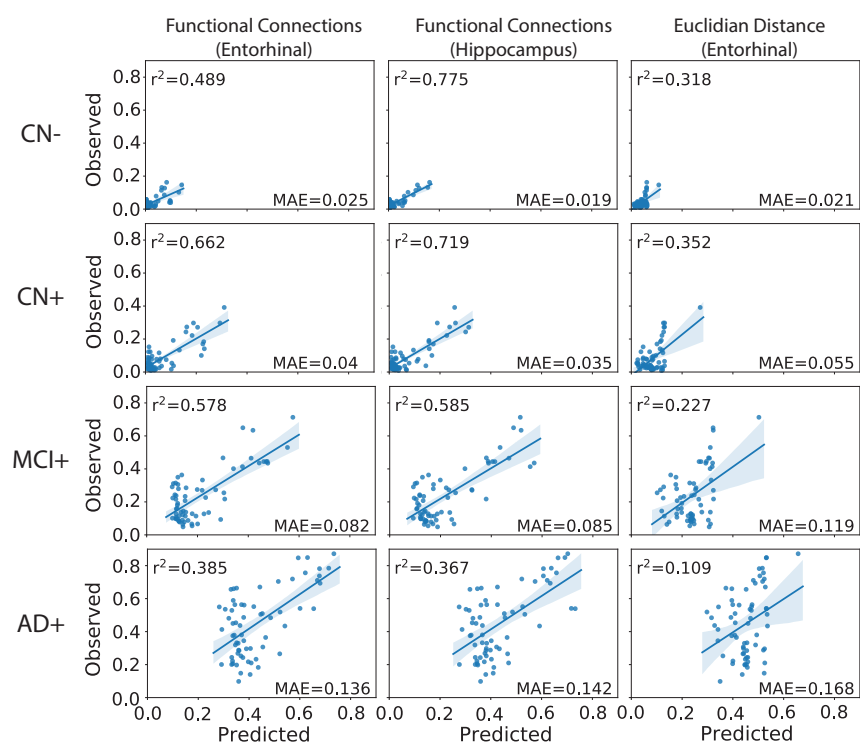


Figure 5: Breakdown of ESM performance by clinical diagnosis. The average performance of three different models are shown separately for CN-, CN+, MCI+ and AD+ diagnostic groups. Remarkable model accuracy was observed in cognitively normal subjects, particularly those without substantial amyloid burden, despite very low levels of overall tau burden. Model accuracy decreased as disease severity increased

319 3.3. Low-level tau spreading is evident and predictable in healthy aging

320 We divided our study sample into groups based on clinical diagnosis
321 and amyloid status. This created four groups, amyloid-negative (CN-) and
322 amyloid-positive (CN+) cognitively normal elderly, amyloid-positive MCI
323 (MCI+) patients and amyloid-positive AD dementia (AD+) patients. We
324 examined model accuracy separately within these groups. We found that,
325 across all models, overall model accuracy decreased with increasing disease
326 severity, but remained high for all diagnostic groups (Fig 5). Unexpectedly,
327 model accuracy was best for CN- individuals, despite a low overall tau
328 burden. Despite being sub-threshold, tau-probability values increased sys-
329 tematically in a pattern predicted by brain connectivity, particularly with a
330 hippocampal epicenter. This was validated by examining model fit against

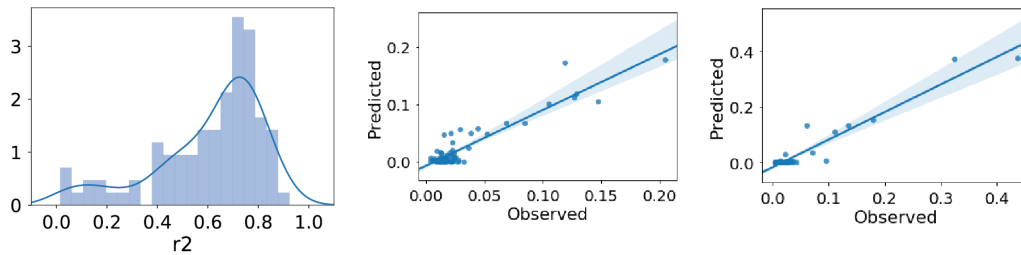


Figure 6: Excellent model performance in CN- individuals. (Left) The distribution of r^2 values representing the range in individual-level model fit across all CN- subjects. Two exemplary subjects are plotted: (middle) a subject with somewhat higher than average tau burden; (right) a subject with low tau burden. Even at very low (subthreshold) levels, the distribution of tau is predicted by functional connectivity patterns.

331 the tau pattern of individual CN- subjects, where the model performed well
332 in CN- subjects with medium or even very low regional tau burden (Fig 6).

333 3.4. Regional β -Amyloid is associated with region model performance

334 For each model, regions-of-interest were classified as either overestimated
335 or underestimated by the model based on the sign of the residual (Fig 7A,B).
336 Underestimated regions are those demonstrating greater tau burden than
337 would be expected given connectivity to the model epicenter (i.e. observed
338 $>$ predicted), while overestimated regions demonstrate less tau than would be
339 expected given their connectivity profile (i.e. predicted $>$ observed). Com-
340 pared to overestimated regions, underestimated regions had greater global
341 β -amyloid burden (Figure, $t = 4.77$, $p = 0.00002$, Fig 7D), suggesting the
342 regional presence of amyloid may accelerate the spread or expression of tau
343 tangles. However, this effect was only present in amyloid+ individuals, and
344 was stronger in individuals with clinical cognitive impairment (Fig 7E).

345 4. Discussion

346 Observations in post-mortem human brains [27, 26] and experiments in
347 animal models [20, 21, 22, 23, 12] have together provided evidence that tau
348 can be transmitted from cell to cell through neuronal projections. However,
349 post-mortem studies cannot provide direct evidence of cell-to-cell spread, and
350 while animal models have proven tau can spread through neuronal connec-
351 tions under certain conditions, they cannot prove that this phenomenon does

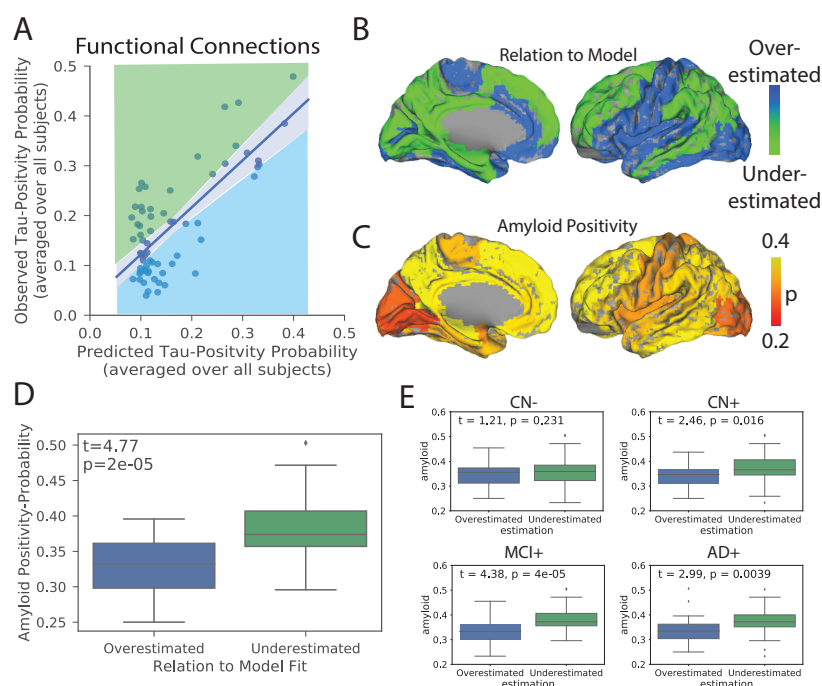


Figure 7: Amyloid explains regional model underestimation. A) Regions were classified as overestimated or underestimated based on the sign of the residual in a comparison of predicted vs. observed values. B) A surface render showing the spatial distribution of over- and underestimated regions. C) A surface render showing the spatial distribution of regional amyloid-positive probabilities. D) Underestimated regions tended to have significantly greater amyloid burden, suggesting these regions had more tau than would be predicted given their connectivity to the model epicenter. E) The same relationship stratified by clinical diagnosis.

352 occur in humans. Studies searching for evidence of tau cell-to-cell transmis-
 353 sion in living humans have been limited by small datasets, simplistic models
 354 and issues relating to the quantitative measurement of tau. Here, we used a
 355 mixture-modeling approach on a large sample of humans on the Alzheimer’s
 356 disease spectrum to enhance the quantification of tau signal, and we applied
 357 to this data a diffusion model based on theoretical principles of an agent
 358 propagating through a network. These simulations explained a majority of
 359 the variance in the global spatial distribution of tau-PET signal in the brain,
 360 and performed nearly equally well in predicting the distribution of tau-PET
 361 signal in individual subjects. A similar model testing the hypothesis that tau

362 spreads across neighboring brain regions was less successful at explaining the
363 overall pattern. While these simulations greatly support the notion that tau
364 spreads through connected neurons in humans, the models performed best in
365 cognitively unimpaired individuals, and also systematically underestimated
366 the magnitude of tau in regions classically shown to harbor β -amyloid. To-
367 gether, these results suggests a model where tau spreads slowly through the
368 limbic network in normal aging, but that the presence of β -amyloid leads to
369 acceleration of tau tangle expression in isocortical regions.

370 Brain networks may be key to the evolution of neurodegenerative dis-
371 ease [49]. The atrophy patterns of many neurodegenerative dementias have
372 been shown to resemble resting-state functional brain networks [50, 51], and
373 network "hubs" are especially vulnerable to neurodegeneration across brain
374 disorders [52]. Studies modeling the diffusion of gray matter degeneration
375 across brain networks have recreated such patterns with impressive accuracy
376 [51, 39, 38]. However, in many neurodegenerative disorders, brain atrophy is
377 preceded and perhaps caused by the aggregation of pathological agents. In
378 Alzheimer's disease, the presence of tau is closely linked to [7, 8], and likely
379 precedes [8, 11], gray matter atrophy. However, because gray matter degen-
380 eration observed in Alzheimer's dementia may be caused by many sources
381 other than Alzheimer's pathology, gray matter degeneration itself cannot be
382 used as proxy for tau (e.g. [53]). PET studies therefore provide a unique
383 advantage by measuring pathological proteins more directly, and employing
384 network diffusion models to PET data has, for example, lead to the success-
385 ful description of the spatial progression of β -amyloid in Alzheimer's disease
386 [37]. Our model uses a similar framework to simulate the spread of tau
387 through the brain and reaches a similar level of success, both within-subject
388 as well as globally across all subjects. The application of network models to
389 other forms of dementia will be needed to conclude whether the spread of
390 pathological proteins through connected neurons is a common thread linking
391 many diseases.

392 While our model recapitulated the early stages of tau spreading accu-
393 rately, later stages were modeled less accurately, with a systematic underes-
394 timation of tau in regions prone to early and high-volume β -amyloid aggre-
395 gation. While tau, not β -amyloid, seems to be the main driver of atrophy in
396 Alzheimer's disease, the commonly-observed concurrence of extra-limbic tau
397 and cortical amyloid burden has lead to speculation that β -amyloid may ac-
398 celerate or otherwise facilitate the spread of tau outside the medial temporal
399 lobe. Recent studies in mice have shown that β -amyloid creates an envi-

400 ronment facilitating the rapid fibrilization of tau [12, 13]. Our data support
401 this notion, as brain regions harboring more β -amyloid, such as the posterior
402 cingulate and precuneus, had a higher incidence of abnormal tau than would
403 be predicted simply by their regional connectivity to the medial temporal
404 lobe. Further supporting this conclusion was the observation that this effect
405 was only seen in amyloid-positive individuals. A conclusive model of tau
406 spreading may not be complete without incorporating dynamic interaction
407 with β -amyloid.

408 Tau tangles are a pathological hallmark of AD, but they are neither spe-
409 cific to AD, nor to neurodegenerative disease in general. The process of aging
410 appears to lead inevitably to the accumulation of tau tangles in the medial
411 temporal lobe and occasionally beyond, a phenomenon known as primary
412 age-related tauopathy (PART) [9], and evidence for the longitudinal accu-
413 mulation of tangles in healthy elderly has been observed [11]. While PART
414 may result in subtle effects on cognition and brain health [54], there is still
415 debate as to whether PART and AD are distinct processes [55]. We show
416 that even in cognitively normal elderly without significant amyloid burden
417 and very low (subthreshold) tau-PET signal, the spatial pattern of tau can
418 be predicted by functional connectivity to medial temporal lobe structures.
419 These findings suggest that even in PART, tau likely spreads from cell to cell
420 through communicating neurons. The results also suggest closer scrutiny of
421 subthreshold tau-PET signal in cognitively unimpaired, amyloid-negative in-
422 dividuals. Elevated SUVR values occurring in a consistent pattern in specific
423 limbic regions may be indicative of very low tau pathology.

424 While our findings lend strong support to the hypothesis of tau spreading
425 through communicating neurons, connectivity patterns and regional amyloid
426 burden together could not fully explain the observed pattern of tau-PET
427 across the brain. While a portion of this discrepancy may be explained by
428 measurement error, there are likely other factors at play. Recent work has
429 outlined a consistent genomic profile across regions that express tau [56], im-
430 plicating regional variation in intrinsic molecular environment may mediate
431 the presence and rate of tau tangle formation. This may explain why, for ex-
432 ample, many subcortical regions do not show substantial tau burden despite
433 connections to regions expressing neurofibrillary tau tangles. In addition, it
434 is also possible that only certain neuron types can facilitate the transmission
435 of tau, which may be challenging to model using macroscopic measures of
436 functional connectivity. Finally, some studies have suggested the directional
437 flow of neuronal activity may influence the spread of brain pathology [57].

438 Future studies incorporating this information, along with dynamics related
439 to regional amyloid burden and regional vulnerability, may achieve a more
440 complete model of tau spreading. However, at present, we show that the
441 spread of tau is predicted by connectivity patterns to a degree that greatly
442 exceeds both chance and other hypotheses of tau spread, and does so in a
443 parsimonious fashion, greatly supporting the notion that connectivity is in
444 some way involved in the spread of tau through the human brain.

445 Tau-PET signal has been notoriously hard to analyze due to extensive
446 off-target binding reducing signal-to-noise ratio (for review, see [29]). We
447 partially circumvented this well-known issue by applying Gaussian mixture-
448 models separately to each region-of-interest. This approach effectively es-
449 tablished a region-specific baseline representing the normal distribution of
450 off-target signal, allowing the identification of outliers expressing SUVR val-
451 ues exceeding the normal expected range. A similar approach has been
452 applied to the spatial staging of brain amyloid, leading to results that were
453 highly consistent across samples [43]. However, this approach used a sin-
454 gle threshold for all regions, whereas our approach was executed separately
455 across each region, thereby accounting for regional ligand dynamics. The
456 conversion of tau-PET SUVR values to tau-positive probabilities resulted in
457 a clean distribution of values across the brain that greatly resembled the
458 progressive pattern described in the pathology literature, and validated the
459 expectation of no substantial burden in the striatum. By both treating each
460 ROI separately but also expressing values along a standardized 0-1 probabil-
461 ity scale, we were able achieve greater regional sensitivity for the detection
462 of both low-level tau, as well as high confidence tangle aggregation. Import-
463 tantly, this approach did not require any arbitrary threshold (e.g. [58] and
464 resulted in discreet probability values, and therefore may benefit future stud-
465 ies or clinical evaluations seeking to classify regions as "tau-positive" with a
466 given level of confidence.

467 Our study comes with a number of limitations. The premise of testing the
468 hypothesis of tau spread through communicating neurons requires that both
469 neuronal connection and tau burden are accurately measured. We attempt
470 to partially surmount these issues by introducing a data-driven approach for
471 overcoming off-target and non-specific binding in AV1451-PET data, and
472 by validating our findings over different connectomes across different sam-
473 ples and modalities. In addition, our mixture-modeling strategy is sensitive
474 to sample size and composition. While it is unlikely that this phenomenon
475 strongly affected the present findings, it is an important point worth con-

476 sideration for future studies utilizing this approach to transform tau-PET
477 data. Another limitation is raised by our choice to remove regions that do
478 not demonstrate measurable tau burden, namely subcortical regions, from
479 the model altogether. Certain subnuclei of subcortical structures such as the
480 thalamus do accumulate tau pathology in Alzheimer’s disease [59], though
481 we were unable to detect such pathology, perhaps due to the resolution of
482 our measurements. While it is possible that subcortical structures partici-
483 pate in neuronal transmission of pathology without expressing the pathology
484 itself, the current implementation of our model does not support this type
485 of dynamic. However, while incidental measurement of indirect functional
486 connectivity is a common critique of functional MRI, here it may pose an
487 advantage, as functional connectivity mediated by subcortical connections
488 may still be present in functional connectomes used for this study.

489 5. Conclusion

490 Altogether, our data strongly supports the notion that tau pathology it-
491 self, or information leading to the the expression of pathology, is transmitted
492 from cell to cell in humans, principally through neuronal connections, and not
493 extracellular space. Our findings further suggest that this phenomenon pro-
494 ceeds slowly but perhaps ubiquitously in normal aging, and that the process
495 is accelerated dramatically in specific brain regions demonstrating β -amyloid
496 burden. While our *in vivo* results cannot prove that tau spreads through neu-
497 ronal connections, we show that more highly connected regions have a higher
498 tendency to be affected closer in time by tau along a specific network path
499 cascading from the medial temporal lobe. Future models may be able to
500 improve results by incorporating region-specific vulnerability factors, direc-
501 tional flow and amyloid dynamics, though contributing such information in
502 a parsimonious way presents a difficult challenge.

503 6. Disclosures

504 OH has acquired research support (for the institution) from Roche, GE
505 Healthcare, Biogen, AVID Radiopharmaceuticals, Fujirebio, and Euroim-
506 mun. In the past 2 years, he has received consultancy/speaker fees (paid
507 to the institution) from Biogen, Roche, and Fujirebio.

508 7. Acknowledgements

509 We would like to thank Bratislav Mistic, Pierre Bellec and Mallar Chakravarty
510 for comments and suggestions during the formulation of this work. JWV is
511 supported by government of Canada through the tri-council Vanier Canada
512 Graduate Doctoral Fellowship. Work at the authors research center was
513 supported by the European Research Council, the Swedish Research Council,
514 the Knut and Alice Wallenberg foundation, the Marianne and Marcus
515 Wallenberg foundation, the Strategic Research Area MultiPark (Multidis-
516 ciplinary Research in Parkinsons disease) at Lund University, the Swedish
517 Alzheimer Foundation, the Swedish Brain Foundation, The Parkinson founda-
518 tion of Sweden, The Parkinson Research Foundation, the Skne Univer-
519 sity Hospital Foundation, and the Swedish federal government under the
520 ALF agreement. Doses of 18F-flutemetamol injection were sponsored by GE
521 Healthcare. The precursor of 18F-flortaucipir was provided by AVID radio-
522 pharmaceuticals. Data collection and sharing for this project was funded by
523 the Alzheimer's Disease Neuroimaging Initiative (ADNI) (National Institutes
524 of Health Grant U01 AG024904) and DOD ADNI (Department of Defense
525 award number W81XWH-12-2-0012). ADNI is funded by the National In-
526 stitute on Aging, the National Institute of Biomedical Imaging and Bioengi-
527 neering, and through generous contributions from the following: AbbVie,
528 Alzheimer's Association; Alzheimer's Drug Discovery Foundation; Araclon
529 Biotech; BioClinica, Inc.; Biogen; Bristol-Myers Squibb Company; CereSpir,
530 Inc.; Cogstate; Eisai Inc.; Elan Pharmaceuticals, Inc.; Eli Lilly and Com-
531 pany; EuroImmun; F. Hoffmann-La Roche Ltd and its affiliated company
532 Genentech, Inc.; Fujirebio; GE Healthcare; IXICO Ltd.; Janssen Alzheimer
533 Immunotherapy Research Development, LLC.; Johnson Johnson Pharma-
534 ceutical Research Development LLC.; Lumosity; Lundbeck; Merck Co.,
535 Inc.; Meso Scale Diagnostics, LLC.; NeuroRx Research; Neurotrack Tech-
536 nologies; Novartis Pharmaceuticals Corporation; Pfizer Inc.; Piramal Imag-
537 ing; Servier; Takeda Pharmaceutical Company; and Transition Therapeutics.
538 The Canadian Institutes of Health Research is providing funds to support
539 ADNI clinical sites in Canada. Private sector contributions are facilitated
540 by the Foundation for the National Institutes of Health (www.fnih.org). The
541 grantee organization is the Northern California Institute for Research and
542 Education, and the study is coordinated by the Alzheimer's Therapeutic
543 Research Institute at the University of Southern California. ADNI data
544 are disseminated by the Laboratory for Neuro Imaging at the University of

545 Southern California.

- 546 [1] V. L. Villemagne, V. Doré, S. C. Burnham, C. L. Masters, C. C. Rowe, Imaging tau
547 and amyloid- β proteinopathies in Alzheimer disease and other conditions, *Nature*
548 *Reviews Neurology* 14 (2018) 225–236.
- 549 [2] V. L. Villemagne, S. Burnham, P. Bourgeat, B. Brown, K. A. Ellis, O. Salvado,
550 C. Szoeki, S. L. Macaulay, R. Martins, P. Maruff, D. Ames, C. C. Rowe, C. L.
551 Masters, Amyloid β deposition, neurodegeneration, and cognitive decline in sporadic
552 Alzheimer’s disease: A prospective cohort study, *The Lancet Neurology* 12 (2013)
553 357–367.
- 554 [3] T. Hedden, H. Oh, A. P. Younger, T. A. Patel, Meta-analysis of amyloid-cognition
555 relations in cognitively normal older adults, *Neurology* 80 (2013) 1341–1348.
- 556 [4] M. C. Donohue, R. A. Sperling, R. Petersen, C. K. Sun, M. Weiner, P. S. Aisen,
557 Association between elevated brain amyloid and subsequent cognitive decline among
558 cognitively normal persons, *JAMA - Journal of the American Medical Association*
559 317 (2017) 2305–2316.
- 560 [5] S. Palmqvist, M. Schöll, O. Strandberg, N. Mattsson, E. Stomrud, H. Zetterberg,
561 K. Blennow, S. Landau, W. Jagust, O. Hansson, Earliest accumulation of β -amyloid
562 occurs within the default-mode network and concurrently affects brain connectivity,
563 *Nature Communications* 8 (2017).
- 564 [6] B. A. Gordon, A. McCullough, S. Mishra, T. M. Blazey, Y. Su, J. Christensen,
565 A. Dincer, K. Jackson, R. C. Hornbeck, J. C. Morris, B. M. Ances, T. L. Benzinger,
566 Cross-sectional and longitudinal atrophy is preferentially associated with tau rather
567 than amyloid β positron emission tomography pathology, *Alzheimer’s and Dementia: Diagnosis, Assessment and Disease Monitoring* 10 (2018) 245–252.
- 569 [7] C. Xia, S. J. Makaretz, C. Caso, S. McGinnis, S. N. Gomperts, J. Sepulcre, T. Gomez-
570 Isla, B. T. Hyman, A. Schultz, N. Vasdev, K. A. Johnson, B. C. Dickerson, Association
571 of In Vivo [18 F]AV-1451 Tau PET Imaging Results With Cortical Atrophy and Symptoms in Typical and Atypical Alzheimer Disease, *JAMA Neurology*
572 74 (2017) 427.
- 574 [8] A. Bejanin, D. R. Schonhaut, R. L. Joie, J. H. Kramer, S. L. Baker, N. Sosa,
575 N. Ayakta, A. Cantwell, M. Janabi, M. Lauriola, J. P. O’neil, M. L. Gorno-Tempini,
576 Z. A. Miller, H. J. Rosen, B. L. Miller, W. J. Jagust, G. D. Rabinovici, Tau pathol-
577 ogy and neurodegeneration contribute to cognitive impairment in Alzheimer’s disease,
578 *Brain* (2017) 1–15.
- 579 [9] J. F. Crary, J. Q. Trojanowski, J. A. Schneider, J. F. Abisambra, E. L. Abner,
580 I. Alafuzoff, S. E. Arnold, J. Attems, T. G. Beach, E. H. Bigio, N. J. Cairns, D. W.
581 Dickson, M. Gearing, L. T. Grinberg, P. R. Hof, B. T. Hyman, K. Jellinger, G. A.
582 Jicha, G. G. Kovacs, D. S. Knopman, J. Kofler, W. A. Kukull, I. R. Mackenzie,

- 583 E. Masliah, A. McKee, T. J. Montine, M. E. Murray, J. H. Neltner, I. Santa-Maria,
584 W. W. Seeley, A. Serrano-Pozo, M. L. Shelanski, T. Stein, M. Takao, D. R. Thal,
585 J. B. Toledo, J. C. Troncoso, J. P. Vonsattel, C. L. White, T. Wisniewski, R. L. Wolt-
586 jer, M. Yamada, P. T. Nelson, Primary age-related tauopathy (PART): a common
587 pathology associated with human aging, *Acta Neuropathologica* 128 (2014) 755–766.
- 588 [10] H. Braak, K. Del Tredici, The preclinical phase of the pathological process underlying
589 sporadic Alzheimer’s disease, *Brain* 138 (2015) 2814–2833.
- 590 [11] T. M. Harrison, R. La Joie, A. Maass, S. L. Baker, K. Swinnerton, L. Fenton, T. J.
591 Mellinger, L. Edwards, J. Pham, B. L. Miller, G. D. Rabinovici, W. J. Jagust, Lon-
592 gitudinal tau accumulation and atrophy in aging and Alzheimers disease, *Annals of*
593 *Neurology* (2018) 229–240.
- 594 [12] Z. He, J. L. Guo, J. D. McBride, S. Narasimhan, H. Kim, L. Changolkar, B. Zhang,
595 R. J. Gathagan, C. Yue, C. Dengler, A. Stieber, M. Nitla, D. A. Coulter, T. Abel,
596 K. R. Brunden, J. Q. Trojanowski, V. M.-y. Lee, Amyloid- β plaques enhance
597 Alzheimer’s brain tau-seeded pathologies by facilitating neuritic plaque tau aggre-
598 gation, *Nature Medicine* 24 (2018) 29–38.
- 599 [13] R. E. Bennett, S. L. DeVos, S. Dujardin, B. Corjuc, R. Gor, J. Gonzalez, A. D. Roe,
600 M. P. Frosch, R. Pitstick, G. A. Carlson, B. T. Hyman, Enhanced Tau Aggregation
601 in the Presence of Amyloid β , *American Journal of Pathology* 187 (2017) 1601–1612.
- 602 [14] E. E. Congdon, E. M. Sigurdsson, Tau-targeting therapies for Alzheimer disease,
603 *Nature Reviews Neurology* 14 (2018) 399–415.
- 604 [15] H. Braak, E. Braak, Neuropathological stageing of Alzheimer-related changes., *Acta*
605 *neuropathologica* 82 (1991) 239–59.
- 606 [16] H. Cho, J. Y. Choi, M. S. Hwang, Y. J. Kim, H. M. Lee, H. S. Lee, J. H. Lee, Y. H.
607 Ryu, M. S. Lee, C. H. Lyoo, In vivo cortical spreading pattern of tau and amyloid
608 in the Alzheimer’s disease spectrum, *Annals of Neurology* (2016) 1–12.
- 609 [17] H. Cho, H. S. Lee, J. Y. Choi, J. H. Lee, Y. H. Ryu, M. S. Lee, C. H. Lyoo, Predicted
610 sequence of cortical tau and amyloid- β deposition in Alzheimer disease spectrum,
611 *Neurobiology of Aging* 68 (2018) 76–84.
- 612 [18] M. Goedert, D. S. Eisenberg, R. A. Crowther, Propagation of Tau Aggregates and
613 Neurodegeneration, *Annual Review of Neuroscience* 40 (2017) 189–210.
- 614 [19] B. Frost, M. I. Diamond, Prion-like mechanisms in neurodegenerative diseases, *Na-*
615 *ture Reviews Neuroscience* 11 (2010) 155–159.
- 616 [20] A. De Calignon, M. Polydoro, M. Su??rez-Calvet, C. William, D. H. Adamowicz,
617 K. J. Kopeikina, R. Pitstick, N. Sahara, K. H. Ashe, G. A. Carlson, T. L. Spires-
618 Jones, B. T. Hyman, Propagation of Tau Pathology in a Model of Early Alzheimer’s
619 Disease, *Neuron* 73 (2012) 685–697.

- 620 [21] L. Liu, V. Drouet, J. W. Wu, M. P. Witter, S. A. Small, C. Clelland, K. Duff, Trans-
621 synaptic spread of tau pathology in vivo, *PLoS ONE* 7 (2012) 1–9.
- 622 [22] M. Iba, J. L. Guo, J. D. McBride, B. Zhang, J. Q. Trojanowski, V. M.-Y. Lee,
623 Synthetic Tau Fibrils Mediate Transmission of Neurofibrillary Tangles in a Transgenic
624 Mouse Model of Alzheimer’s-Like Tauopathy, *Journal of Neuroscience* 33 (2013)
625 1024–1037.
- 626 [23] F. Clavaguera, H. Akatsu, G. Fraser, R. A. Crowther, S. Frank, J. Hench, A. Probst,
627 D. T. Winkler, J. Reichwald, M. Staufenbiel, B. Ghetti, M. Goedert, M. Tolnay,
628 Brain homogenates from human tauopathies induce tau inclusions in mouse brain,
629 *Proceedings of the National Academy of Sciences* 110 (2013) 9535–9540.
- 630 [24] J. A. Miller, S. Horvath, D. H. Geschwind, Divergence of human and mouse brain
631 transcriptome highlights Alzheimer disease pathways, *Proceedings of the National*
632 *Academy of Sciences* 107 (2010) 12698–12703.
- 633 [25] E. Drummond, T. Wisniewski, Alzheimer’s disease: experimental models and reality.,
634 *Acta neuropathologica* 133 (2017) 155–175.
- 635 [26] S. L. DeVos, B. T. Corjuc, D. H. Oakley, C. K. Nobuhara, R. N. Bannan, A. Chase,
636 C. Commins, J. A. Gonzalez, P. M. Dooley, M. P. Frosch, B. T. Hyman, Synaptic
637 tau seeding precedes tau pathology in human Alzheimer’s disease brain, *Frontiers in*
638 *Neuroscience* 12 (2018) 1–15.
- 639 [27] J. Brettschneider, K. Del Tredici, V. M. Lee, J. Q. Trojanowski, Spreading of pathol-
640 ogy in neurodegenerative diseases: A focus on human studies, *Nature Reviews Neu-*
641 *roscience* 16 (2015) 109–120.
- 642 [28] J. Y. Choi, H. Cho, S. J. Ahn, J. H. Lee, Y. H. Ryu, M. S. Lee, C. H. Lyoo, “Off-
643 Target” ¹⁸F-AV-1451 Binding in the Basal Ganglia Correlates with Age-
644 Related Iron Accumulation, *Journal of Nuclear Medicine* (2017) jnumed.117.195248.
- 645 [29] L. Lemoine, A. Leuzy, K. Chiotis, E. Rodriguez-Vieitez, A. Nordberg, Tau positron
646 emission tomography imaging in tauopathies: The added hurdle of off-target binding,
647 *Alzheimer’s and Dementia: Diagnosis, Assessment and Disease Monitoring* 10 (2018)
648 232–236.
- 649 [30] M. Marquié, M. Siao Tick Chong, A. Antón-Fernández, E. E. Verwer, N. Sáez-
650 Calveras, A. C. Meltzer, P. Ramanan, A. C. Amaral, J. Gonzalez, M. D. Normandin,
651 M. P. Frosch, T. Gómez-Isla, [F-18]-AV-1451 binding correlates with postmortem
652 neurofibrillary tangle Braak staging, *Acta Neuropathologica* (2017) 1–10.
- 653 [31] S. N. Lockhart, N. Ayakta, J. R. Winer, R. La Joie, G. D. Rabinovici, W. J. Jagust,
654 Elevated (18)F-AV-1451 PET tracer uptake detected in incidental imaging findings.,
655 *Neurology* 88 (2017) 1095–1097.

- 656 [32] D. T. Jones, J. Graff-Radford, V. J. Lowe, H. J. Wiste, J. L. Gunter, M. L. Senjem,
657 H. Botha, K. Kantarci, B. F. Boeve, D. S. Knopman, R. C. Petersen, C. R. Jack, Tau,
658 Amyloid, and Cascading Network Failure across the Alzheimers disease Spectrum,
659 Cortex (2017) 1–17.
- 660 [33] J. W. Vogel, N. Mattsson, Y. Iturria-Medina, O. T. Strandberg, M. Schöll,
661 C. Dansereau, S. Villeneuve, W. M. van der Flier, P. Scheltens, P. Bellec, A. C.
662 Evans, O. Hansson, R. Ossenkoppele, Data-driven approaches for tau-PET imaging
663 biomarkers in Alzheimer’s disease, Human Brain Mapping (2018) 638–651.
- 664 [34] T. E. Cope, T. Rittman, R. J. Borchert, P. S. Jones, D. Vatansever, K. Allinson,
665 L. Passamonti, P. Vazquez Rodriguez, W. R. Bevan-Jones, J. T. O’Brien, J. B. Rowe,
666 Tau burden and the functional connectome in Alzheimer’s disease and progressive
667 supranuclear palsy, Brain 141 (2018) 550–567.
- 668 [35] N. Franzmeier, A. Rubinski, J. Neitzel, Y. Kim, A. Damm, D. L. Na, H. J. Kim,
669 C. H. Lyoo, H. Cho, S. Finsterwalder, M. Duering, S. W. Seo, M. Ewers, Functional
670 connectivity associated with tau levels in ageing, Alzheimers, and small vessel disease,
671 Brain (2019) 1–15.
- 672 [36] H. I. Jacobs, T. Hedden, A. P. Schultz, J. Sepulcre, R. D. Perea, R. E. Amariglio,
673 K. V. Papp, D. M. Rentz, R. A. Sperling, K. A. Johnson, Structural tract alterations
674 predict downstream tau accumulation in amyloid-positive older individuals, Nature
675 Neuroscience 21 (2018) 424–431.
- 676 [37] Y. Iturria-Medina, R. C. Sotero, P. J. Toussaint, A. C. Evans, Epidemic Spread-
677 ing Model to Characterize Misfolded Proteins Propagation in Aging and Associated
678 Neurodegenerative Disorders, PLoS Computational Biology 10 (2014).
- 679 [38] Y.-Q. Zheng, Y. Zhang, Y. H. C. Yau, Y. Zeighami, K. Larcher, B. Mistic, A. Dagher,
680 Connectome architecture, gene expression and functional co-activation shape the
681 propagation of misfolded proteins in neurodegenerative disease, bioRxiv (2018)
682 449199.
- 683 [39] A. Raj, A. Kuceyeski, M. Weiner, A Network Diffusion Model of Disease Progression
684 in Dementia, Neuron 73 (2012) 1204–1215.
- 685 [40] S. Palmqvist, H. Zetterberg, N. Mattsson, P. Johansson, L. Minthon, K. Blennow,
686 M. Olsson, O. Hansson, Detailed comparison of amyloid PET and CSF biomarkers
687 for identifying early Alzheimer disease, Neurology 85 (2015) 1240–1249.
- 688 [41] O. Hansson, M. J. Grothe, T. O. Strandberg, T. Ohlsson, Tau Pathology Distribution
689 in Alzheimer’s disease Corresponds Differentially to Cognition-Relevant Functional
690 Brain Networks 11 (2017).
- 691 [42] R. S. Desikan, F. Ségonne, B. Fischl, B. T. Quinn, B. C. Dickerson, D. Blacker, R. L.
692 Buckner, A. M. Dale, R. P. Maguire, B. T. Hyman, M. S. Albert, R. J. Killiany, An

- 693 automated labeling system for subdividing the human cerebral cortex on MRI scans
694 into gyral based regions of interest, *NeuroImage* 31 (2006) 968–980.
- 695 [43] M. J. Grothe, H. Barthel, J. Sepulcre, M. Dyrba, O. Sabri, S. J. Teipel, Alzheimer’s
696 Disease Neuroimaging Initiative, In vivo staging of regional amyloid deposition.,
697 *Neurology* 0 (2017).
- 698 [44] S. Palmqvist, H. Zetterberg, K. Blennow, S. Vestberg, U. Andreasson, D. J. Brooks,
699 R. Owenius, D. Hägerström, P. Wollmer, L. Minthon, O. Hansson, Accuracy of
700 Brain Amyloid Detection in Clinical Practice Using Cerebrospinal Fluid β -Amyloid
701 42, *JAMA Neurology* 71 (2014) 1282.
- 702 [45] P. Bellec, COBRE preprocessed with NIAK 0.17 - lightweight release, 2016.
- 703 [46] Y. Iturria-Medina, E. J. Canales-Rodríguez, L. Melie-García, P. A. Valdés-Hernández,
704 E. Martínez-Montes, Y. Alemán-Gómez, J. M. Sánchez-Bornot, Characterizing brain
705 anatomical connections using diffusion weighted MRI and graph theory, *NeuroImage*
706 36 (2007) 645–660.
- 707 [47] Y. Iturria-Medina, F. M. Carbonell, R. C. Sotero, F. Chouinard-Decorte, A. C. Evans,
708 Multifactorial causal model of brain (dis)organization and therapeutic intervention:
709 Application to Alzheimer’s disease, *NeuroImage* 152 (2017) 60–77.
- 710 [48] M. Schöll, S. N. Lockhart, D. R. Schonhaut, J. P. O’Neil, M. Janabi, R. Ossenkoppele,
711 S. L. Baker, J. W. Vogel, J. Faria, H. D. Schwimmer, G. D. Rabinovici, W. J. Jagust,
712 PET Imaging of Tau Deposition in the Aging Human Brain, *Neuron* 89 (2016) 971–
713 982.
- 714 [49] Y. Iturria-Medina, A. C. Evans, On the central role of brain connectivity in neurode-
715 generative disease progression., *Frontiers in aging neuroscience* 7 (2015) 90.
- 716 [50] W. W. Seeley, R. K. Crawford, J. Zhou, B. L. Miller, M. D. Greicius, Neurode-
717 generative Diseases Target Large-Scale Human Brain Networks, *Neuron* 62 (2009)
718 42–52.
- 719 [51] J. Zhou, E. D. Gennatas, J. H. Kramer, B. L. Miller, W. W. Seeley, Predicting
720 Regional Neurodegeneration from the Healthy Brain Functional Connectome, *Neuron*
721 73 (2012) 1216–1227.
- 722 [52] N. A. Crossley, A. Mechelli, J. Scott, F. Carletti, P. T. Fox, P. McGuire, E. T.
723 Bullmore, The hubs of the human connectome are generally implicated in the anatomy
724 of brain disorders, *Brain* 137 (2014) 2382–2395.
- 725 [53] J. Torok, P. D. Maia, F. Powell, S. Pandya, A. Raj, A method for inferring regional
726 origins of neurodegeneration, *Brain* 141 (2018) 863–876.

- 727 [54] K. S. Jefferson-George, D. A. Wolk, E. B. Lee, C. T. McMillan, Cognitive decline
728 associated with pathological burden in primary age-related tauopathy, *Alzheimer's*
729 *and Dementia* 13 (2017) 1048–1053.
- 730 [55] H. Braak, K. Del Tredici, Are cases with tau pathology occurring in the absence of
731 $A\beta$ deposits part of the AD-related pathological process?, *Acta Neuropathologica*
732 128 (2014) 767–772.
- 733 [56] M. J. Grothe, J. Sepulcre, G. Gonzalez-Escamilla, I. Jelic, M. Schöll, O. Hans-
734 son, S. J. Teipel, Molecular properties underlying regional vulnerability to Alzheimers
735 disease pathology, *Brain* (2018) 2755–2771.
- 736 [57] M. Scherr, L. Utz, M. Tahmasian, L. Pasquini, M. J. Grothe, J. P. Rauschecker,
737 T. Grimmer, A. Drzezga, C. Sorg, V. Riedl, Effective connectivity in the default mode
738 network is distinctively disrupted in Alzheimer's disease-A simultaneous resting-state
739 FDG-PET/fMRI study, *Human Brain Mapping* (2019) 1–10.
- 740 [58] C. R. Jack, H. J. Wiste, S. D. Weigand, T. M. Therneau, V. J. Lowe, D. S. Knopman,
741 J. L. Gunter, M. L. Senjem, D. T. Jones, K. Kantarci, M. M. Machulda, M. M. Mielke,
742 R. O. Roberts, P. Vemuri, D. A. Reyes, R. C. Petersen, Defining imaging biomarker
743 cut points for brain aging and Alzheimer's disease, *Alzheimer's and Dementia* 13
744 (2017) 205–216.
- 745 [59] J. P. Aggleton, A. Pralus, A. J. D. Nelson, M. Hornberger, Thalamic pathology and
746 memory loss in early Alzheimers disease: moving the focus from the medial temporal
747 lobe to Papez circuit, *Brain* 139 (2016) 1877–1890.